

## RESEARCH ARTICLE

# Propionic acid and not caproic acid, attenuates nonalcoholic steatohepatitis and improves (cerebro) vascular functions in obese *Ldlr*<sup>-/-</sup>.Leiden mice

Anouk C. Tengeler<sup>1</sup> | Eveline Gart<sup>2,3</sup> | Maximilian Wiesmann<sup>1</sup> | Ilse A. C. Arnoldussen<sup>1</sup> | Wim van Duyvenvoorde<sup>2</sup> | Marloes Hoogstad<sup>1</sup> | Pieter J. Dederen<sup>1</sup> | Vivienne Verweij<sup>1</sup> | Bram Geenen<sup>1</sup> | Tamas Kozicz<sup>1,4</sup> | Robert Kleemann<sup>1,5</sup> | Martine C. Morrison<sup>2,3</sup> | Amanda J. Kiliaan<sup>1</sup>

<sup>1</sup>Department of Anatomy, Donders Institute for Brain, Cognition and Behavior, Preclinical Imaging Centre, Radboud University Medical Center, Nijmegen, the Netherlands

<sup>2</sup>Department of Metabolic Health Research, The Netherlands Organisation for Applied Scientific Research (TNO), Leiden, the Netherlands

<sup>3</sup>Human and Animal Physiology, Wageningen University, Wageningen, the Netherlands

<sup>4</sup>Department of Biochemistry and Molecular Biology, Mayo Clinic, Rochester, MN, USA

<sup>5</sup>Department of Vascular Surgery, Leiden University Medical Center, Leiden, the Netherlands

## Correspondence

Amanda J. Kiliaan, Department of Anatomy, Radboud University Medical Center, Donders Institute for Brain,

## Abstract

The obesity epidemic increases the interest to elucidate impact of short-chain fatty acids on metabolism, obesity, and the brain. We investigated the effects of propionic acid (PA) and caproic acid (CA) on metabolic risk factors, liver and adipose tissue pathology, brain function, structure (by MRI), and gene expression, during obesity development in *Ldlr*<sup>-/-</sup>.Leiden mice. *Ldlr*<sup>-/-</sup>.Leiden mice received 16 weeks either a high-fat diet (HFD) to induce obesity, or chow as reference group. Next, obese HFD-fed mice were treated 12 weeks with (a) HFD + CA (CA), (b) HFD + PA (PA), or (c) a HFD-control group. PA reduced the body weight and systolic blood pressure, lowered fasting insulin levels, and reduced HFD-induced liver macrovesicular steatosis, hypertrophy, inflammation, and collagen content. PA increased the amount of glucose transporter type 1-positive cerebral blood vessels, reverted cerebral vasoreactivity, and HFD-induced effects in microstructural gray and white matter integrity of optic tract, and somatosensory and visual cortex. PA and CA also reverted HFD-induced effects in functional connectivity between visual and auditory cortex. However, PA mice were more anxious in open field, and showed reduced activity of synaptogenesis and glutamate regulators in hippocampus. Therefore, PA treatment

**Abbreviations:** ASL, arterial spin labeling; B2M, B2-microglobulin; BOLD, blood oxygen level dependent; CA, caproic acid; CBF, cerebral blood flow; CE, cholesteryl ester; CLS, crown-like structures; COX, cytochrome c oxidase; CS, citrate synthase; DAB-Ni, diaminobenzidine-nickel; DCX, doublecortin; DTI, diffusion tensor imaging; DVC, digital ventilated cages; FA, fractional anisotropy; FAIR, flow-sensitive alternating inversion recovery; FAS, fatty acid synthase; FC, free cholesterol; GAPDH, glyceraldehyde 3-phosphate dehydrogenase; GLUT-1, glucose transporter 1; gWAT, gonadal white adipose tissue; HE, hematoxylin-eosin; HFD, high-fat diet; IBA-1, ionized calcium-binding adapter molecule 1; IHC, Immunohistochemistry; IPA, Ingenuity Pathway Analysis; *Ldlr*<sup>-/-</sup>, low-density lipoprotein receptor knockout; MD, mean diffusivity; mWAT, mesenteric white adipose tissue; MWM, morris water maze; NAFLD, nonalcoholic fatty liver disease; NASH, nonalcoholic steatohepatitis; NMDA, n-methyl-d-aspartate; PA, propionic acid; PSD-95, post-synaptic density-95; rs-fMRI, resting-state functional MRI; SAA, serum amyloid A; SBP, systolic blood pressure; SCC, succinate cytochrome c oxidoreductase; SCFA, short-chain fatty acid; sWAT, subcutaneous white adipose tissue; SYP1, synaptophysin; TG, triglyceride; WAT, white adipose tissue.

Anouk C. Tengeler and Eveline Gart are share first authorship.

Martine C. Morrison and Amanda J. Kiliaan are share last authorship.

This is an open access article under the terms of the Creative Commons Attribution-NonCommercial License, which permits use, distribution and reproduction in any medium, provided the original work is properly cited and is not used for commercial purposes.

© 2020 The Authors. *The FASEB Journal* published by Wiley Periodicals LLC on behalf of Federation of American Societies for Experimental Biology

Cognition & Behaviour, Preclinical Imaging Centre PRIME, Geert Grooteplein Noord 21, Nijmegen 6525 EZ, the Netherlands.  
Email: Amanda.Kiliaan@radboudumc.nl

#### Funding information

TNO early research program 'Body Brain Interactions'

should be used with caution even though positive metabolic, (cerebro) vascular, and brain structural and functional effects were observed.

#### KEYWORDS

cerebral vasoreactivity, cognition, liver fibrosis, neuroimaging, obesity

## 1 | INTRODUCTION

The prevalence of obesity has increased considerably worldwide over the past decades.<sup>1</sup> Obesity is associated with ectopic fat accumulation, dyslipidemia, hyperinsulinemia, and it promotes the development of nonalcoholic fatty liver disease (NAFLD).<sup>2</sup> NAFLD encompasses a spectrum of liver disease, ranging from simple steatosis to the more severe stage of nonalcoholic steatohepatitis (NASH). NASH is characterized by steatosis and lobular inflammation,<sup>3,4</sup> and can progress to liver fibrosis.<sup>5</sup> Other than modifying lifestyle factors, for instance weight loss through dietary advice and physical activity, no approved pharmacological therapy is yet available for NASH. In addition to the dysfunction of peripheral metabolic organs, obesity is also associated with mitochondrial dysfunction and alterations in brain structure and cognitive dysfunction.<sup>6,7</sup> Obesity-associated changes in white matter have been reported in numerous studies<sup>8-10</sup> and effects on the cerebrovasculature, that is, decreased cerebral vasoreactivity and glucose transporter 1 (GLUT-1) expression, a marker for vascular endothelium cells and vascular health.<sup>11,12</sup>

Short-chain fatty acids (SCFAs) have already shown some beneficial effects on obesity development. For example, CA has been reported to have possible antilipogenic effects.<sup>13-16</sup> Moreover, a small-scale clinical study showed that an elevation of colonic PA levels was associated with reduced weight gain and reductions in liver lipids.<sup>17</sup> In rodent studies, PA has been shown to protect against diet-induced obesity.<sup>18-21</sup> Furthermore, elevated PA levels were associated with reduced visceral adiposity and steatohepatitis in obese mice that were treated with fructo-oligosaccharides.<sup>22</sup>

Herein, we investigated whether CA and PA can attenuate the development of HFD-induced obesity and associated NASH, liver fibrosis and associated brain dysfunction on functional and structural level. To do so, we used the low-density lipoprotein receptor knockout (Ldlr<sup>-/-</sup>). Leiden mice which develop dyslipidemia, hyperinsulinemia, obesity, NASH, liver fibrosis, and hypertension in conjunction with brain dysfunction in a period of about 30 weeks on HFD.<sup>6,23</sup> PA and CA were administered as dietary supplement in a therapeutic setting, that is, after a 16-week run-in to establish obesity.

## 2 | MATERIALS AND METHODS

### 2.1 | Mice, diets, and study design

This was a randomized and blinded (blinded for investigators and outcome assessors) controlled study. Male Ldlr<sup>-/-</sup>. Leiden mice were obtained from a specific pathogen-free breeding stock at TNO Metabolic Health Research (Leiden, the Netherlands) and were housed in the Preclinical Imaging Center (PRIME) at the Animal Research Facility, Radboudumc Nijmegen, the Netherlands. Mice were group-housed in digital ventilated cages (DVC; Tecniplast SPA, Buguggiate (VA) Italy) in which locomotor activity of the mice can be tracked 24 hours/day. Mice were housed in conventional animal rooms (relative humidity 50%-60%, temperature 21°C, light cycle 7 AM-7 PM), 2-3 mice per cage with ad libitum access to food and water. All animal experiments were carried out in accordance with international European ethical standards (European Directive 2010/63/EU) and were approved by the TNO Animal Welfare Body (Permit number: TNO-345) and the Veterinary Authority of the Radboud university medical center (Radboudumc; Permit number: RU-DECnonbreakingspace2017-0063-002). All applicable (inter)national, and institutional guidelines for the care and use of animals were followed and are reported herein in accordance with the ARRIVE guidelines.<sup>24</sup>

The study design of this experiment is shown in Figure 1A. From weaning at 3 weeks of age onward, all groups received a standard chow diet (9.0% kcal fat, 58.0% carbohydrates, and 33.0% kcal protein Sniff R/M-H diet V1530, Sniff Spezialdiäten GmbH, Soest, Germany). At 15 weeks of age, mice were divided into 4 experimental groups (N = 15 per group) that were matched for body weight prior to treatment. Mice in group 1 were kept on the chow diet, and mice in group 2-4 were switched to an HFD (45.0% kcal fat, 35.0% carbohydrates and 20.0% kcal protein, D12451, Research Diets Inc, New Brunswick, USA) with anise. From 31 weeks of age until the end of the study (for a total of 12 weeks), group 3 HFD was supplemented with 2.5% w/w CA (CA mice), and group 4 with 2.5% w/w PA (PA mice).

Food intake at cage level and individual body weight were monitored weekly. Blood samples were collected before and after 8 weeks of treatment. Systolic blood pressure, cognition with the Morris water maze test (MWM),

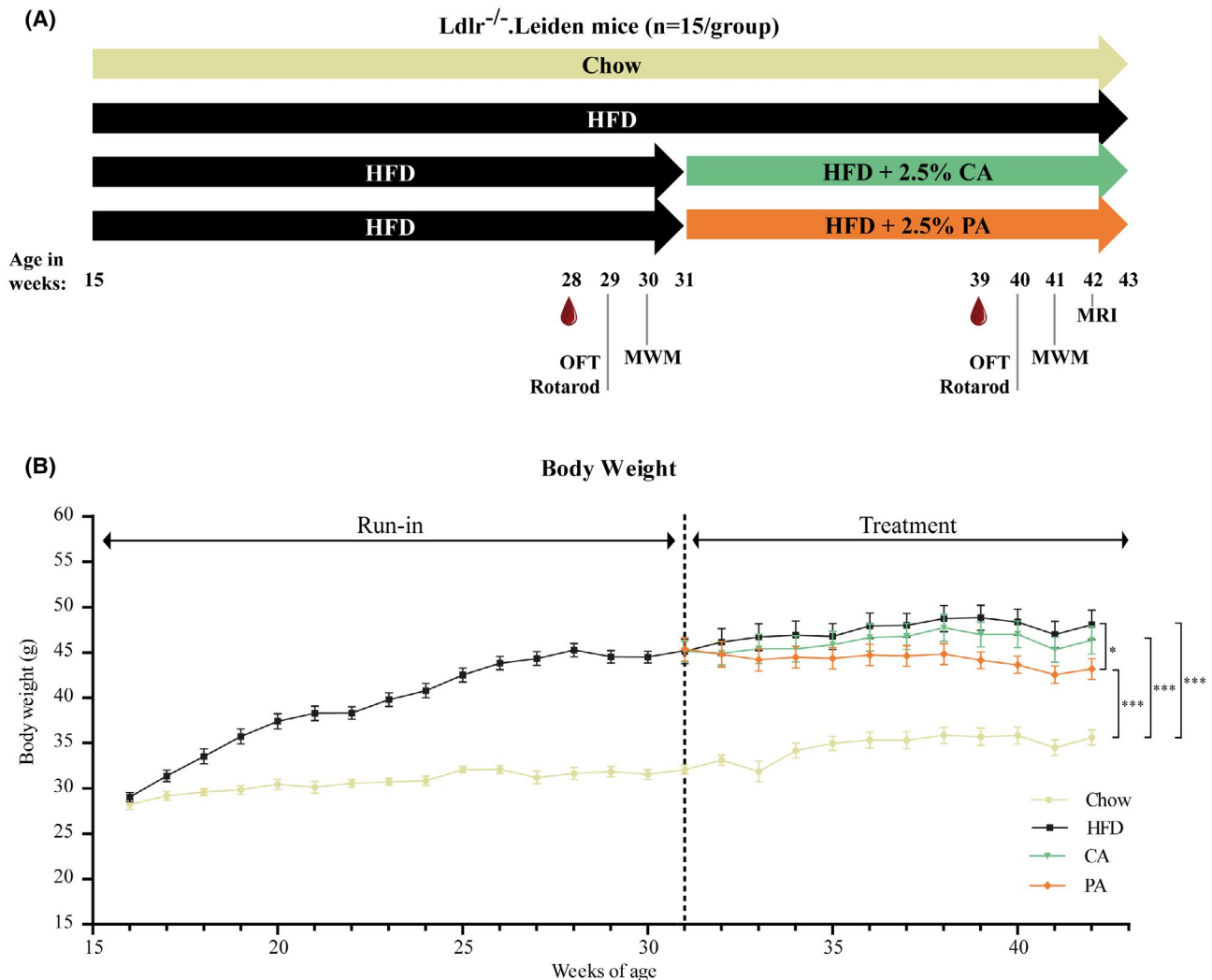


**FIGURE 1** Study design and body weight. A, Study design. From 15 to 30 weeks of age,  $Ldlr^{-/-}$  mice received either a chow diet or an HFD diet. At 31 weeks of age CA and PA treatment started. Systolic blood pressure was measured, and plasma samples were collected (see droplet). Behavior and cognition were assessed, and MRI-experiments were performed. In week 43, all mice were sacrificed via cervical dislocation followed by decapitation. B, Body weight. An HFD supplemented with CA or PA started at 31 weeks of age. Reference mice were kept on chow. HFD: high-fat diet; PA: propionic acid; CA: caproic acid; OFT: Open Field test; MWM: Morris water maze. Data are presented as mean  $\pm$  SEM. \* $P < .05$ ; \*\*\* $P < .001$ . N = 14 (HFD) or N = 15 (chow, CA, PA) mice per group

behavior in an Open Field Test and motor skills with the Rotarod experiment were assessed before treatment and after 9-10 weeks of treatment. Brain function and structure were measured using magnetic resonance imaging (MRI) after 11 weeks of treatment. After 12 weeks, mice were sacrificed via cervical dislocation followed by decapitation. One HFD-mouse was sacrificed early in the study due to health concerns resulting from fighting, and was, therefore, excluded from all analyses.

## 2.2 | Plasma measurements

Blood samples were collected after 5 hours fast via tail vein bleeding to determine whole blood glucose, and for isolation

of EDTA plasma in which total cholesterol, triglycerides, serum amyloid A (SAA), and insulin were determined as described previously.<sup>23</sup>

## 2.3 | Systolic blood pressure

SBP was measured using a computerized and warmed tail-cuff plethysmography device (IITC Life Scientific Instruments, Woodland Hill, CA, USA). One trial, consisting of 10 measurements, was used to habituate the mice to the restrainer and acclimatize the animals to the complete procedure. SBP was then measured for a total of 20 measurements, in two trials on two consecutive days and expressed as mean SBP in millimeter of mercury (mm Hg).

## 2.4 | Liver histological and biochemical analyses

The liver was isolated and weighed. Development of NAFLD was analyzed in the medial liver lobe in 3  $\mu\text{m}$  liver hematoxylin-eosin (HE) stained sections by a board-certified pathologist using a well-established rodent NASH scoring method adapted from the human NAFLD activity score (NAS).<sup>23,25</sup> Briefly, the level of total steatosis or hypertrophy (abnormally enlarged hepatocytes) per mouse was expressed as a percentage of the total liver section affected. Hepatic inflammation was quantified by counting the number of inflammatory aggregates in five fields per mouse at 100x magnification (field of view 4.15  $\text{mm}^2$ ) and expressed as the number of foci per  $\text{mm}^2$ .

The sinister lobe was snap-frozen in liquid nitrogen and stored at  $-80^\circ\text{C}$  for biochemical analyses. Hepatic total collagen content was determined with a hydroxyproline assay (Quickzyme, Leiden, the Netherlands) and protein with a total protein assay (Quickzyme) according to the manufacturer's instructions. The hepatic ketone body  $\beta$ -hydroxybutyrate was measured with a colorimetric assay kit (Cayman chemical, Michigan, USA) and protein content was assayed with (Pierce BCA protein assay kit, Thermo Fisher Scientific, Waltham, USA) in an assay buffer containing protease inhibitors (100  $\text{mg}/\text{mL}$ ) following the manufacturer's protocol.

Liver lipids were determined in a 100  $\text{mg}/\text{mL}$  phosphate-buffered saline homogenate following the Bligh and Dyer method,<sup>26</sup> then separated by high-performance thin-layer chromatography on silica gel plates. Subsequently, the lipids were stained as described previously,<sup>23</sup> and analyzed with ChemiDoc Touch Imaging System (Bio-Rad, Hercules, USA). Liver triglyceride (TG), cholesterol ester (CE), and free cholesterol (FC) content was quantified using Image-lab version 5.2.1 software (Bio-Rad, Hercules, USA) and expressed per  $\text{mg}$  liver protein. In the same liver homogenates, the glycogen content was determined according to the manufacturer's protocol (MAK016 Glycogen assay kit, Sigma-Aldrich, Steinheim, Germany).

## 2.5 | White adipose tissue (WAT) analyses

Gonadal (gWAT), mesenteric (mWAT), and subcutaneous (sWAT) WAT depots were isolated, weighed, and 5  $\mu\text{m}$  paraffin embedded sections were stained with hematoxylin-phloxine-saffron and scanned for digital analysis (Aperio AT2, Leica Biosystems, Amsterdam, the Netherlands). Size of adipose cells were analyzed using Adiposoft<sup>27</sup> an open-source automated plug-in for the image processing package Fiji<sup>28</sup> for ImageJ.<sup>29</sup> Inflammation was quantified by counting the number of crown-like structures (CLS; the histological hallmark of adipose tissue inflammation<sup>30</sup> in the same fields

used for adipocyte size analysis and expressed as number of CLS per 1000 adipocytes.

## 2.6 | Digital ventilated cages (DVC)

Mice were housed in DVC cages (2-3 mice per cage) during the experiment to study locomotor activity 24 hours/day. Activity was monitored via 12 electrodes underneath the home-cage, as described previously.<sup>31,32</sup> For analysis of the processed results, we used activity data of 2 days and 2 nights before the start of the interventions, and 2 days and 2 nights at the end of the experiment. Activity measures were corrected for the number of mice per cage.

## 2.7 | Rotarod

To study sensory-motor integration mice were placed on a rotating rod (3.18 cm in diameter; IITC Inc, Woodland Hills, CA, USA) and their ability to remain on the device was recorded as latency to fall. First, mice were accustomed to the task by placing them on a stationary rod for 1 minute followed by a test trial at 10 rpm. Next, four accelerating trials with intervals of 30 minutes were performed (4 to 40 rpm) with a maximum duration of 300 seconds.

## 2.8 | Open field

Explorative behavior and locomotion were assessed in the open field test. Mice were placed individually in a square open field (45 cm  $\times$  45 cm  $\times$  30 cm) with transparent Plexiglas walls, and recorded for 10 minutes. Locomotion and explorative behavior were automatically calculated with EthoVision XT10.1 (Noldus, Wageningen, the Netherlands).

## 2.9 | Morris water maze

The MWM was used to examine long-term memory and spatial learning abilities. During the acquisition phase, the mice were trained to find the platform in a circular pool (diameter 108 cm) that was filled with water ( $21\text{--}22^\circ\text{C}$ ), made opaque by adding milk powder. The platform (diameter 8 cm) was submerged 1 cm below the water surface and located in the North-East quadrant of the pool. Mice performed 4 acquisition trials per day starting from four different positions (South, North, East, West; maximal swimming time 120 s; 30 s on the platform; inter-trial interval 60 min) during four consecutive days. Visual cues were present on the four walls surrounding the pool at a distance of 0.5 m. All trials were recorded and latency to find the platform (s) was used as a

measure for spatial learning. Mice performed a single probe trial at the end of day 4 of acquisition, in which the platform was removed from the pool.

During this probe trial, the mice were allowed to swim freely for 120 seconds. Trials were recorded and analyzed with EthoVision XT 10.1.

## 2.10 | Functional and structural brain experiments using MRI

All MRI measurements were performed using an 11.7-T BioSpec Avance III small animal MR system (Bruker BioSpin, Ettlingen, Germany). Isoflurane (Abbott Animal Health, Abbott Park, IL, USA) was used for anesthesia (3.5% for induction and ~1.7% for maintenance) in a 1:2 oxygen and air mixture). Imaging parameters can be found in Table S1.

Arterial spin labeling (ASL) was assessed to indicate cerebral blood flow (CBF) levels using an established ASL method with flow-sensitive alternating inversion recovery (FAIR) technique.<sup>33</sup> To induce vasoconstriction, the normal 1:2 oxygen-air mixture was changed to a 3:0 oxygen and air mixture. CBF values from both conditions were used to evaluate the ability of the cerebrovasculature to adapt from a normal condition to a vasoconstrictive condition, which is referred to as cerebral vasoreactivity.<sup>34</sup> Cerebral vasoreactivity was calculated by subtraction of the vasoconstriction CBF from the normal CBF values, and this was then divided by the sum of the normal and vasoconstrictive CBF values. To calculate regional CBF we used the same protocol as described previously.<sup>35</sup> CBF was measured in the total brain, cortex, thalamus (an important brain structure for relaying motor signals to the cortex), and the hippocampus (an important brain structure for memory consolidation).

To investigate white and gray matter integrity in the brain, diffusion tensor imaging (DTI) was employed as described.<sup>36,37</sup> Fractional anisotropy is a marker of the degree of myelination and fiber density of white matter, while mean diffusivity characterizes an inverse measure of the membrane density.<sup>38</sup> These scalars were measured in several manually selected white matter and gray matter areas: fornix and corpus callosum, and regions in the left and right hemisphere: auditory cortex, hippocampus, motor cortex, optic tract, somatosensory cortex, visual cortex, caudate putamen, anterior commissure, amygdala, external capsule, fimbria, forceps minor, and internal capsule.<sup>39</sup>

Resting-state functional MRI (rs-fMRI) acquisition was performed to assess functional connectivity between specific regions of interest (ROI) that support multiple cognitive and motor processes: dorsal hippocampus, ventral hippocampus, auditory cortex, motor cortex, somatosensory cortex, and visual cortex. Functional connectivity between ROIs was calculated from the blood oxygen level-dependent (BOLD) time series using total and partial correlation analyses as

previously described.<sup>36</sup> Partial correlations accentuates the direct connectivity between two ROI while it regresses the temporal BOLD signal from all other ROIs.<sup>36,40</sup>

## 2.11 | Enzymatic mitochondrial activity analysis in brain tissue

A homogenate of snap-frozen cerebellum (N = 8 randomly selected animals per treatment group) was made with a glass-glass potter tube in SEF buffer (0.25 M sucrose, 2 mM K-EDTA, 10 mM phosphate buffer, pH 7.4) to obtain a 5% w/v homogenate. The homogenized samples were centrifuged at 600 g for 10 minutes at 2°C and the supernatant underwent three freeze-thaw cycles to adequately permeabilize the mitochondria. Enzyme activities of the individual complexes of the respiratory chain (complex I, II, III and IV), citrate synthase (CS) and Succinate cytochrome C oxidoreductase (SCC) were measured spectrophotometrically on a KoneLab 20XT analyzer (Thermo Scientific, Waltham, MA, USA), following previously described methods.<sup>41,42</sup> Enzyme activities were normalized to CS activity (a marker for the number of mitochondria<sup>43</sup>).

## 2.12 | Quantitative real-time polymerase chain reaction

Snap-frozen hippocampi were used for mRNA level analysis using quantitative real-time polymerase chain reaction (qRT-PCR) of post-synaptic density-95 (PSD-95) and synaptophysin (SYP-1), as previously described.<sup>44</sup> Glyceraldehyde 3-phosphate dehydrogenase (GAPDH) and  $\beta$ 2-microglobulin (B2M) were used as reference genes. To determine the threshold cycle (CT) values, the StepOne Software version 2.2.2 was used. CT values were normalized against the average of the two reference genes and transformed to the comparative CT values using the Pfaffl method.<sup>45</sup>

## 2.13 | Gene expression analysis using the NanoString neuroinflammation panel

The isolated hippocampal RNA, as used previously for qRT-PCR, concentration was measured spectrophotometrically using a NanoDrop 1000 (Isogen Life Science, De Meern, Netherlands). To assess the quality of the isolated RNA, the 2100 Bioanalyzer (Agilent Technologies, Amstelveen, Netherlands) was used. Molecular barcodes from the nCounter Neuroinflammation panel (XT-CSO-MNROI1-12) code set, included 770 genes and 13 internal reference genes for normalization. The isolated RNA (25ng/ul sample) was used to make a reporter code set master mix and samples from chow, HFD and PA were incubated for 24 hours at 65°C for hybridization

following the manufacturer's protocol. Hybridized samples were then loaded on to an nCounter cartridge and run on the nCounter SPRINT (NanoString Technologies, Seattle, WA, USA) to measure barcode signals. nSolver 4.0 (NanoString Technologies, USA) was used to analyze the geometric mean of internal reference genes was used to compute the reference normalization factor. Internal references with a count below background levels or outside the 0.10-10.0 range normalization factor were excluded. Herein internal reference *Asb10* average count fell below background levels and *Xpnp1* was affected by our treatment, and both had to be excluded from the analyses. Normalized gene expression data were used for gene enrichment analysis across pathways and biological processes with the Ingenuity Pathway Analysis suite (IPA; www.ingenuity.com). The upstream regulator analysis tool of IPA was used to assess the activity of upstream regulators as reported.<sup>46</sup> Briefly, the gene expression levels of all known target genes of an upstream regulator of interest were analyzed together. A Z-score less than  $-2$  indicates a significantly reduced transcriptional activity, while a Z-score greater than  $2$  indicates significant activation based on the direction of gene expression changes of target genes as reported in translational studies.<sup>23</sup>

## 2.14 | Immunohistochemistry on brain tissue

The left brain hemisphere was immersion-fixed overnight at  $4^{\circ}\text{C}$  in 4% paraformaldehyde in 0.1 M PBS, and subsequently stored at  $4^{\circ}\text{C}$  in 0.1 M PBS with 0.01% sodium azide. Coronal frozen brain sections ( $-60^{\circ}\text{C}$ ) were cut in 8 series of 30- $\mu\text{m}$ -thick sections that were used for diaminobenzidine-nickel (DAB-Ni) immunohistochemical (IHC) staining purposes. IHC was performed using standard free-floating labeling procedures, using the protocol described in other studies.<sup>34,44,47</sup>

Brain sections were stained for doublecortin (DCX) as marker for immature neurons (neurogenesis) using polyclonal goat anti-doublecortin (1:8000; sc-8066 Santa Cruz Biotechnology Inc, Santa Cruz, CA, USA). Glucose transporter 1 (GLUT-1) stainings were used to quantify the amount of glucose transporters on brain blood vessels (indication for blood vessel wall integrity) with GLUT-1 polyclonal rabbit anti-GLUT1 (1:80 000; Chemicon International Inc, Temecula, CA, USA). To assess activated microglia (measure for neuroinflammation) ionized calcium-binding adapter molecule 1 (IBA-1) was stained with polyclonal goat anti-IBA1 (1:8000, Abcam, Cambridge, United Kingdom). Secondary antibodies donkey anti-goat biotin (1:1500; Jackson ImmunoResearch, West Grove, PA, USA) and donkey anti-rabbit biotin (1:1500; Jackson ImmunoResearch) were used.

DCX-positive cells were quantified in the hippocampus ( $-1.97$  mm posterior to bregma) in three successive sections per mouse. Stained brain regions were counted at 40x

magnification by two independent observers using a Zeiss Axioscop microscope equipped with hardware and software of MBF Bioscience (Williston, VT, USA). GLUT-1 and IBA-1 positive (+) DAB-Ni immunohistochemistry was scored using ImageJ, in sections photographed with an Axio Imager A2 (Zeiss Germany). Measurements of IBA-1 and GLUT-1 density were defined as the area covered with either (a) relative IBA-1+ or GLUT-1+ staining, or (b) IBA-1+ or GLUT-1+ staining per  $\text{mm}^2$ , all in the cortex, thalamus and hippocampus (bregma  $-1.97$  mm). In addition, the intensity of the GLUT-1 staining was calculated by subtracting the mean particle intensity from 255.<sup>48</sup> Intensity was quantified using ImageJ, in the same regions mentioned above.

## 2.15 | Statistics

The upstream regulators were analyzed using the upstream regulator analysis tool of IPA. All other data were analyzed using IBM SPSS for Windows 25.0 software (SPSS Inc, Chicago, IL, USA), and are expressed as mean  $\pm$  SEM.

Parameters that were measured at multiple separate time points (ie, body weight, caloric intake, and the acquisition of the MWM) were analyzed using repeated measures ANOVA with Bonferroni correction for multiple comparisons. The post hoc Dunnett's multiple comparison two-sided t test was used to compare treatment groups to the HFD control group. In addition, significant effects were also compared to the chow group using the same Dunnett's post hoc test. These results are described in Table S2. To compare treatment groups to the HFD control group and the chow control group, the post hoc Dunnett's multiple comparison two-sided t test was used. When a significant interaction between diet and time was present, the data were split for the concerning factor and analyzed again with repeated measures ANOVA. All other data (behavioral tests, imaging, biochemistry) were analyzed using multivariate ANOVA with Bonferroni correction for multiple comparisons (normally distributed) followed by Dunnett's multiple comparison two-sided t test, or Kruskal-Wallis test (not normally distributed data) followed by a post hoc Mann-Whitney U test to compare groups to the HFD and chow group. Statistical outliers were removed from the dataset. The number of mice that was considered an outlier per test is described in Table S3.

## 3 | RESULTS

### 3.1 | PA attenuates HFD-induced obesity independent of food intake

During the 16-week run-in period, HFD-treated mice gained significantly more weight than the reference mice on chow ( $P < .001$ ; see Figure 1B). After 12 weeks of treatment

these weight gain differences persisted with HFD-fed mice being significantly heavier than chow-fed mice ( $P < .001$ ). Body weight attenuating effects were not observed for CA, whereas PA markedly attenuated HFD-induced body weight gain ( $P < .05$  vs HFD). Average caloric intake was slightly lower in HFD compared to chow ( $P < .05$ , Table 1). Caloric intake between HFD, CA and PA did not differ.

### 3.2 | PA attenuated metabolic risk factors and systolic blood pressure

We next examined the effects of the treatments on metabolic risk factors (Table 1). Plasma cholesterol and triglyceride concentrations were increased by HFD ( $P < .01$ ), and this was not affected by CA or PA. Glucose levels were comparable in all groups (Table 1). Insulin levels were significantly increased by HFD ( $P < .01$ ). CA did not affect plasma insulin, while PA reduced the HFD-induced increase in plasma insulin levels ( $P < .05$ ).

Obesity-associated hypertension was assessed by measuring SBP before and after treatment. HFD-fed mice had a significantly higher SBP than chow-fed mice before the start of CA and PA treatment ( $P < .001$ ) and this difference persisted until the end of the experiment ( $P < .001$ ). CA had no significant effect on SBP, whereas PA lowered the HFD-induced increase in SBP ( $P < .01$ ; Table 1).

Plasma concentrations of SAA, an inflammatory marker produced by inflamed adipose tissue and liver,<sup>49</sup> were low on chow, and significantly increased by HFD ( $P < .001$ ). SAA was unchanged by CA treatment, and PA treatment tended to reduce the HFD-induced increase in SAA levels ( $P = .056$ ).

### 3.3 | PA treatment reduces HFD-induced liver steatosis, inflammation and collagen content

We next studied the liver, which is the first organ SCFAs pass after absorption from the intestine. Liver weight increased on HFD ( $P < .001$ , Figure 2A) and was not affected by CA or PA. HE-stained liver cross-sections were analyzed for histopathological features of NAFLD (Figure 2B). Macrovesicular steatosis (Figure 2C) was hardly present in the chow group, whereas the HFD-fed mice developed pronounced macrovesicular steatosis ( $P < .001$ ). CA treatment did not affect macrovesicular steatosis. In contrast, PA treatment significantly reduced HFD-induced macrovesicular steatosis ( $P < .05$ ). Microvesicular steatosis was also increased in HFD-fed animals (Figure 2D) ( $P < .001$ ), with no effect of CA and a trend reduction by PA ( $P = .08$ ). The cross-sectional area that was covered with abnormally enlarged hepatocytes (hepatocellular hypertrophy; Figure 2E) was strongly increased by HFD ( $P < .05$ ) and this HFD-induced increase was significantly reduced by PA only ( $P < .05$ ). Inflammatory aggregates were practically absent on chow (Figure 2F), whereas HFD livers showed a high number of inflammatory aggregates ( $P < .001$ ). CA did not significantly affect the number of inflammatory aggregates. However, PA reduced the HFD-induced number of inflammatory aggregates ( $P < .01$ ).

Hepatic collagen content was determined as a measure of fibrosis (Figure 2G). The hepatic collagen content was markedly increased by HFD ( $P < .01$ ). Liver fibrosis was not affected by CA, while PA decreased hepatic collagen content ( $P < .01$ ).

Histopathological analyses were supplemented by measurement of liver lipids,  $\beta$ -hydroxybutyrate and glycogen in liver homogenates. Liver lipid analysis of cholesteryl esters

**TABLE 1** Metabolic parameters at the end of the experiment

	Chow	HFD	CA	PA
Body weight (g)	35.61 $\pm$ 0.83	48.04 $\pm$ 1.62***	46.35 $\pm$ 1.54	43.17 $\pm$ 1.13 <sup>&amp;</sup>
Average caloric intake <sup>a</sup> (kcal/day/mouse)	13.77 $\pm$ 0.68	11.52 $\pm$ 0.67*	11.96 $\pm$ 0.45	11.68 $\pm$ 0.24
Cholesterol (mM)	7.36 $\pm$ 0.46	34.78 $\pm$ 2.95***	32.53 $\pm$ 2.64	30.94 $\pm$ 2.16
Triglycerides (mmol/L)	1.71 $\pm$ 0.16	5.70 $\pm$ 0.80***	5.38 $\pm$ 0.89	4.52 $\pm$ 0.94
Glucose (mmol/L)	6.89 $\pm$ 0.33	6.65 $\pm$ 0.34	6.87 $\pm$ 0.21	7.19 $\pm$ 0.14
Insulin(ng/mL)	2.25 $\pm$ 0.47	4.68 $\pm$ 0.63**	4.07 $\pm$ 0.47	3.23 $\pm$ 0.31 <sup>&amp;</sup>
SBP (mm Hg)	107.33 $\pm$ 2.15	126.79 $\pm$ 1.43***	122.27 $\pm$ 2.81	116.93 $\pm$ 1.53 <sup>&amp;</sup>
SAA (ug/mL)	11.30 $\pm$ 0.67	26.94 $\pm$ 2.14***	26.24 $\pm$ 1.67	21.38 $\pm$ 1.45

Note: Data are presented as Mean  $\pm$  SEM.

<sup>a</sup>Average food intake during the 12-week treatment period.

\* $P < .05$ ; \*\* $P < .01$ ; \*\*\* $P < .001$  compared to control. <sup>&</sup> $P < .05$  compared to HFD.

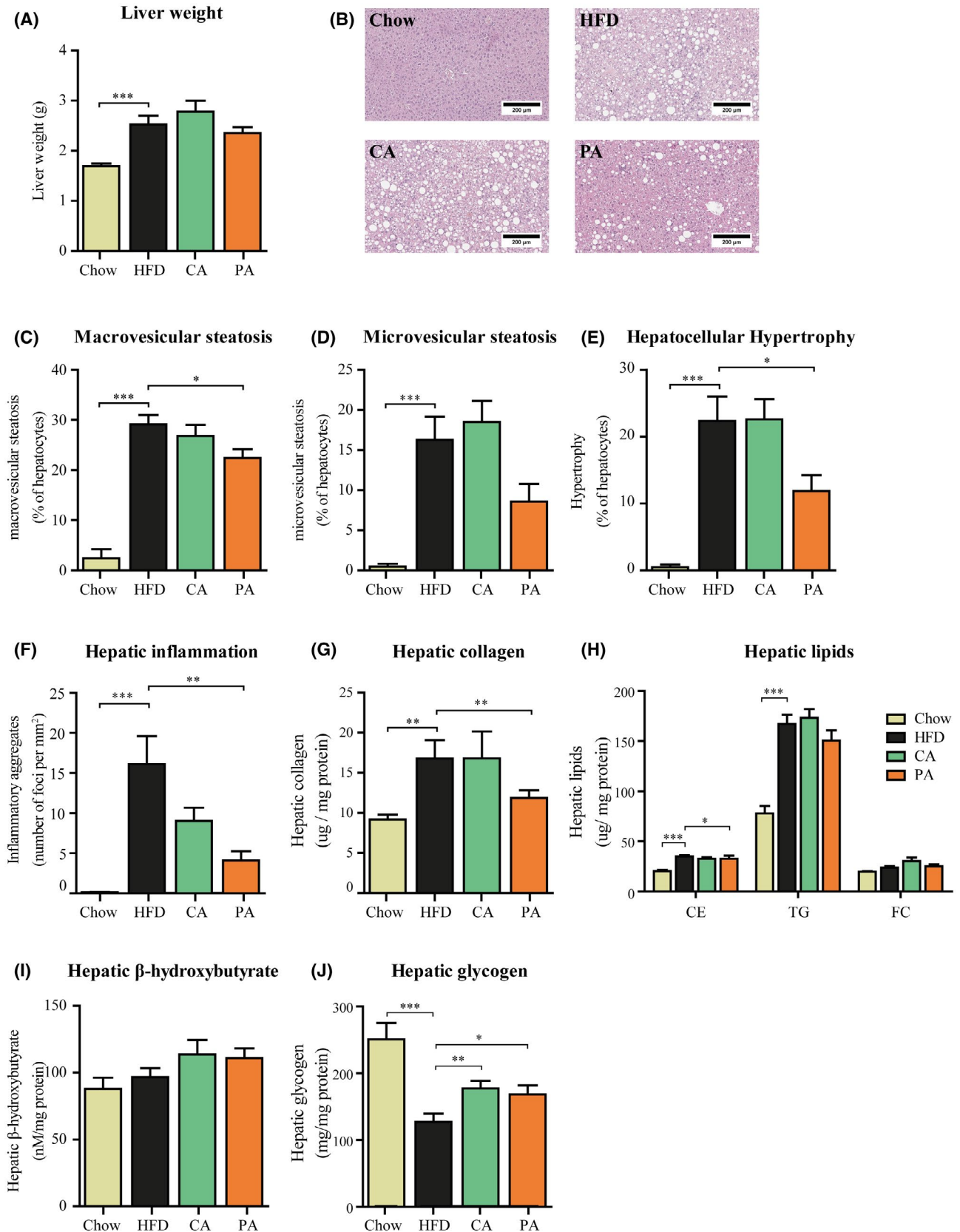


**FIGURE 2** Effect of 12-week treatment with CA and PA on the liver. A, Liver weight, (B) representative images of hematoxylin-eosin stained liver sections, (C) macrovesicular steatosis, (D) microvesicular steatosis, (E) hepatocellular hypertrophy and (F) hepatic inflammation. Liver homogenates were analyzed for (G) collagen content, (H) cholesteryl esters (CE), triglycerides (TG) and free cholesterol (FC), (I) ketone body  $\beta$ -hydroxybutyrate as marker for the rate of  $\beta$ -oxidation and (J) glycogen. HFD: high-fat diet; PA: propionic acid; CA: caproic acid. Data are presented as mean  $\pm$  SEM, \* $P$  < .05 or \*\* $P$  < .01 or \*\*\* $P$  < .001 compared to HFD

(CE), triglycerides (TG), and free cholesterol (FC), showed that CE and TG increased pronouncedly on HFD (CE and TG:  $P < .001$ ; Figure 2H). CA did not alter any of the liver lipids, whereas PA lowered the HFD-induced CE levels ( $P < .05$ ). The concentrations of  $\beta$ -hydroxybutyrate, a ketone body that is formed during beta-oxidation of lipids, were not affected by CA and PA (Figure 2I). Since hepatic steatosis and insulin resistance are associated with impairment of glycogen synthesis,<sup>50</sup> we quantified hepatic glycogen levels (Figure 3J). HFD reduced glycogen levels relative to chow ( $P < .001$ ). The HFD-induced reduction in glycogen levels was partly prevented by CA ( $P < .01$ ) and PA treatment ( $P < .05$ ).

Collectively, these data show that CA had no effect on liver pathology, whereas the attenuating effects of PA on obesity and metabolic risk factors were paralleled by pronounced reductions in NASH and fibrosis.

### 3.4 | PA reduced subcutaneous fat mass and increased the frequency of small adipocytes

Next, we determined whether the observed reduction in body weight with PA was accompanied by an effect on adiposity, adipocyte morphology, and inflammation in different fat depots (Figure 3). sWAT, gWAT, and mWAT weight were increased by HFD treatment (all  $P < .001$  vs chow, Figure 3A-C). CA did not affect the mass of these depots, while PA significantly reduced WAT mass relative to HFD ( $P < .05$ ) and non-significantly lowered mWAT mass relative to HFD ( $P = .08$ ).

Relative to chow, HFD feeding resulted in a shift toward an increased frequency of hypertrophic adipocytes in all three depots (% of adipocytes  $>8000 \mu\text{m}^2$ :  $P < .001$  in sWAT;  $P < .01$  in gWAT and  $P < .001$  in mWAT; Figure 3D-F) with a concomitant reduction in small adipocytes (% of adipocytes  $<2000 \mu\text{m}^2$ :  $P < .001$  in sWAT;  $P < .05$  in mWAT and  $P < .01$  in eWAT; Figure 3D-F). Only PA was able to affect these HFD-induced changes, with an increased frequency of small adipocytes in sWAT ( $2000\text{-}4000 \mu\text{m}^2$ ,  $P < .05$ ) and reduced frequency of hypertrophic adipocytes in mWAT ( $>8000 \mu\text{m}^2$ ;  $P < .05$ ). WAT inflammation, as quantified by the number of crown-like structures (CLS) was practically absent on chow (Figure 3G-I). HFD-feeding increased the number of CLS relative to chow in gWAT ( $P < .001$ ) and mWAT ( $P < .05$ ). CA and PA treatment did not affect CLS counts in these depots relative to HFD.

Taken together, PA had a modest effect on adiposity in sWAT but did not reduce WAT inflammation in sWAT, gWAT or mWAT.

### 3.5 | CA and PA do not affect behavior or spatial memory

Motor coordination was studied with the Rotarod. HFD-fed mice had a lower latency to fall compared to the chow-fed

mice before the start of the interventions ( $P < .001$ ; Figure S1A). At the end of the experiment, HFD still had a lower latency to fall off the rod compared to chow mice ( $P < .001$ ) and this was not affected by CA or PA (Figure 4A).

We did not find differences in exploration or locomotion activity in the open field test before the start of the interventions (Figure S1B) and at the end of the experiment (Figure 4B). However, PA mice spent less time in the periphery and more time in the corners of the open field than chow mice ( $P < .05$ ; Figure 4B), whereas frequency of entering the corners did not differ between groups. This suggests increased anxiety in PA mice. In addition, PA mice showed lower walking velocity and reduced total distance moved than chow mice (Figure S1C,D; Table S2), although no differences between groups were observed in home cage activity during the day or night as monitored in the DVC before the start of the interventions and at the end of the experiment (Figure S2A,B).

Spatial learning and memory of the mice were tested with the MWM test. All mice learned to find the hidden platform and showed a significant learning effect between day 1-2, day 1-3, and day 1-4 ( $P < .001$ ) during the acquisition phase before the start of the treatments (Figure 4C). When the MWM was repeated after 10 weeks of treatment, we similarly found that mice were still able to find the hidden platform after 25-54 seconds with no differences between the treatment groups. Next, a probe test was performed in which the platform of the MWM was removed. No significant effects between treatment groups were observed at the start of the intervention (Figure S1E-G) and at the end of the experiment in mean swimming velocity, the frequency to visit the former platform location, or time spent in the former platform location (Figure 5D-F).

Collectively, these behavioral experiments show that CA and PA were not able to reverse the HFD-induced reduced motor coordination in the rotarod test. Exploration activity and spatial learning and memory were not affected by HFD-feeding and were not affected by CA and PA treatment.

### 3.6 | PA treatment reverts HFD-induced changes in cerebral vasoreactivity

Effects on cerebrovasculature were assessed by measurement of CBF in the cortex, thalamus and hippocampus under normal and vasoconstrictive conditions. These two parameters were then used to calculate cerebral vasoreactivity a measure of the ability to respond to vasoconstrictive stimuli. CBF under normal and vasoconstrictive conditions did not differ between groups in any of the regions assessed (Figure 5A,B). While HFD (relative to chow) and CA (relative to HFD) had no effect on cerebral vasoreactivity, PA significantly improved cerebral vasoreactivity in the cortex

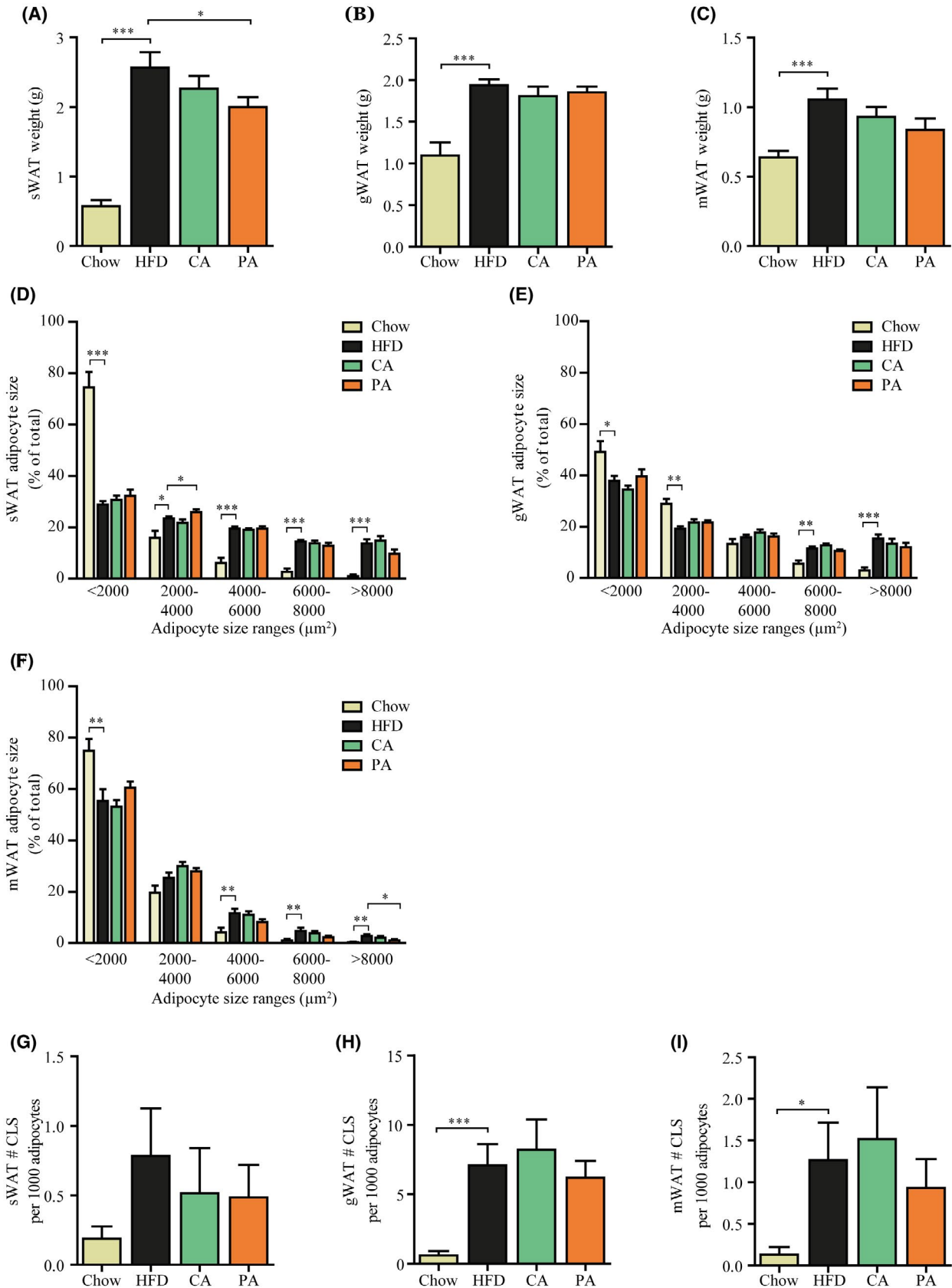


**FIGURE 3** Adipose tissue analysis of subcutaneous (sWAT), gonadal (gWAT), and mesenteric (mWAT) depots after 12 weeks of CA and PA treatment: (A) sWAT (B) gWAT, and (C) mWAT weight. Distribution of adipocyte sizes in (D) sWAT, (E) gWAT, and (F) mWAT. Number of crown-like structures (CLS) per 1000 adipocytes in (G) sWAT, (H) gWAT, and (I) mWAT. HFD: high-fat diet; PA: propionic acid; CA: caproic acid. Data are presented as mean  $\pm$  SEM, \* $P$  < .05 or \*\* $P$  < .01 or \*\*\* $P$  < .001 compared to HFD control

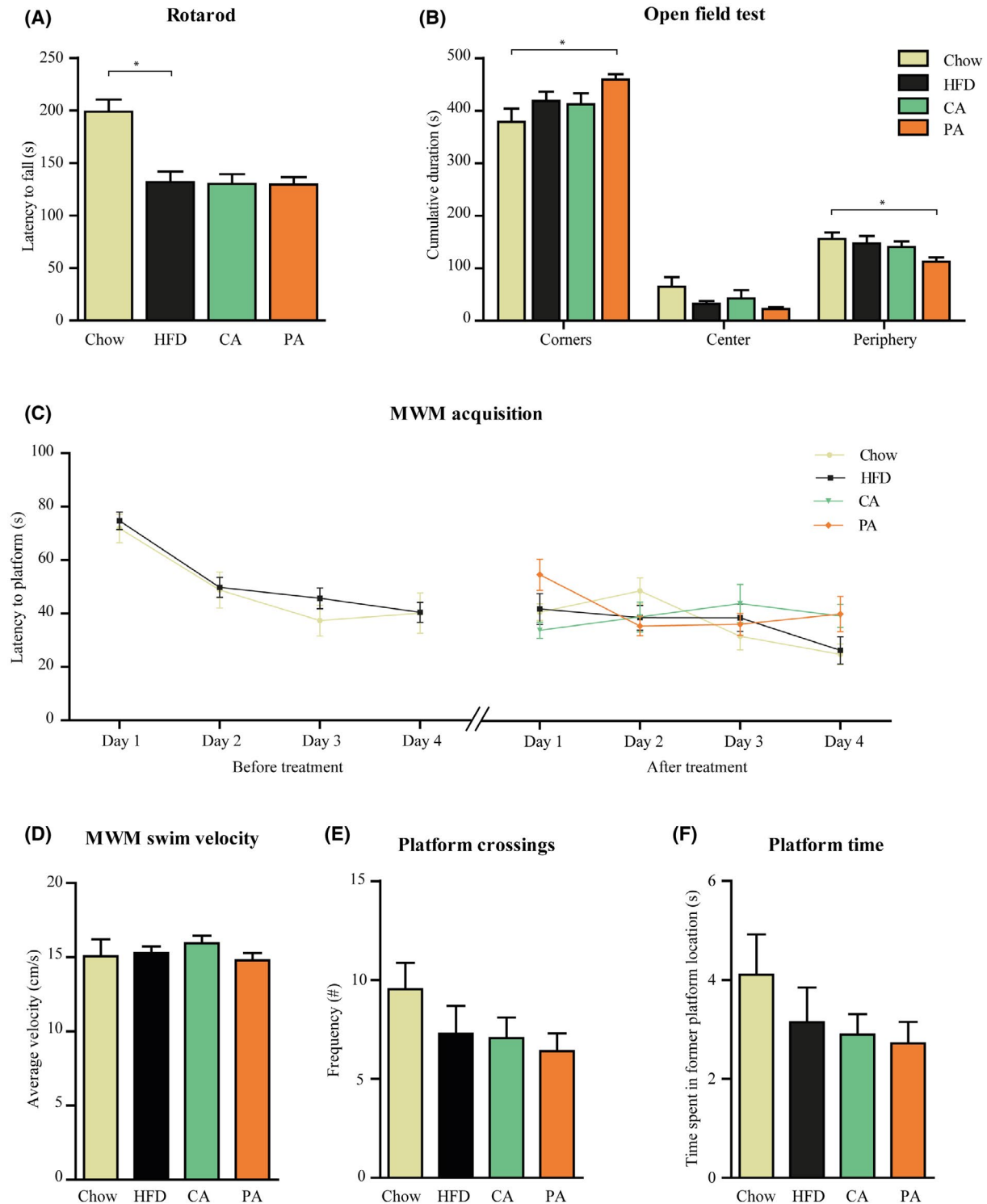


**FIGURE 4** Behavioral and cognitive tests. A, Latency to fall from the rotating rod. B, Cumulative duration(s) spent in corners, periphery and center in the open field test. C, Acquisition test of the Morris water maze (MWM) before and after treatment. The latency to find the platform was measured on 4 consecutive days. D, Mean swim velocity, (E) frequency of crossing the former platform location, and (F) total time spent at the former platform location during the probe test of the MWM. HFD: high-fat diet; PA: propionic acid; CA: caproic acid. Data are presented as mean  $\pm$  SEM, \* $P < .05$ . Open field test:  $N = 14$  (chow and HFD) or  $N = 15$  (CA and PA) per group. MWM and Rotarod:  $N = 14$  (HFD) or  $N = 15$  (chow, CA, PA) mice per group

and hippocampus ( $P < .05$  compared to HFD; Figure 5C) and reverted cerebral vasoreactivity to chow levels ( $P > .05$  compared to chow).

Immunohistochemical stainings were performed to assess neurogenesis (DCX), neuroinflammation (IBA-1), and cerebrovascular integrity (GLUT-1). No differences between

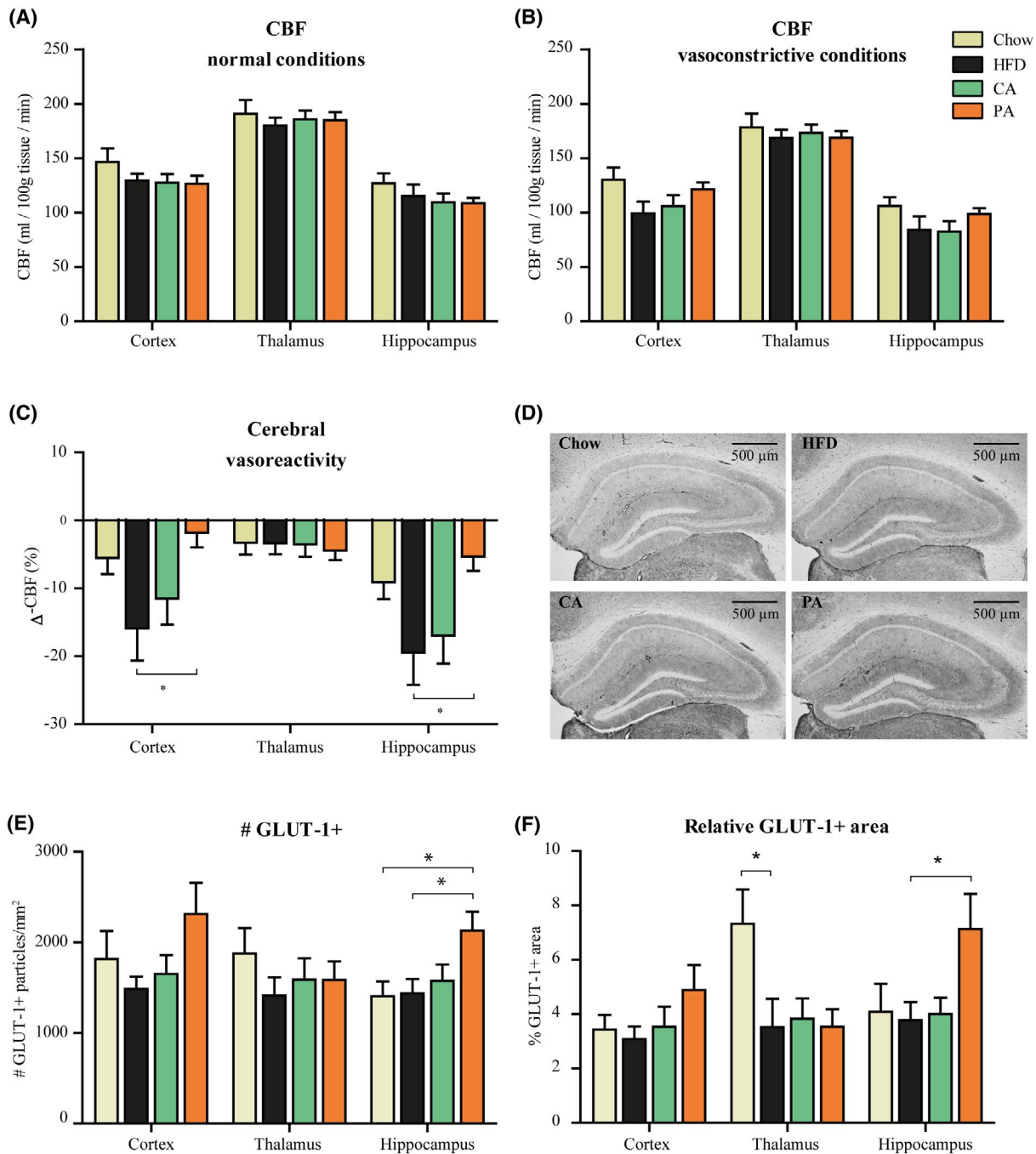


**FIGURE 5** Cerebrovascular parameters. A, Cerebral blood flow (CBF) levels were assessed under normal conditions; and (B) under vasoconstrictive conditions in the cortex, hippocampus, and thalamus. C, Cerebral vasoreactivity was measured using normal and vasoconstrictive CBF, as a measure of ability to respond to vasoconstrictive stimuli (D) Representative images of GLUT-1 staining in Chow, HFD, CA, and PA mice (5 × objective, scale bar represents 500 μm). E, Quantification of the relative GLUT-1+ area, and (F) amount of GLUT-1+ particles per mm<sup>2</sup> in the cortex, hippocampus and thalamus. HFD: high-fat diet; PA: propionic acid; CA: caproic acid; CBF: cerebral blood flow; GLUT-1: glucose transporter type 1. Data are presented as mean ± SEM, \**P* < .05 or \*\**P* < .01 or #*P* < .08. CBF: N = 14 (chow and CA), N = 13 (HFD) and N = 15 (PA). GLUT-1: N = 14 (HFD), N = 14 (chow, CA) or N = 15 (PA) mice per group

groups were observed in the number of DCX+ cells in the hippocampus (Figure S3A). Furthermore, no differences between groups were observed in the amount of IBA-1+ staining or relative IBA-1+ positive area in the cortex, hippocampus or thalamus (Figure S3B,C). HFD-fed mice had a smaller relative GLUT-1+ area in the thalamus than chow-fed

mice (*P* < .05; Figure 5D). CA had no effect, whereas PA increased the GLUT-1+ area (*P* < .05) and the number of GLUT-1+ particles per mm<sup>2</sup> measures for blood vessel density, in the hippocampus (*P* < .05; Figure 5D,E). The number of GLUT-1+ particles per mm<sup>2</sup> was even higher than in chow mice (*P* < .05). GLUT-1 intensity, reflecting the amount of

GLUT-1 transporters, was not affected by HFD (compared to chow) or CA (compared to HFD). However, we observed a trend toward an increased GLUT-1 intensity in PA mice compared to HFD in the cortex ( $P = .056$ ) and hippocampus ( $P = .079$ ). GLUT-1 intensity in PA mice was even higher than in chow mice in the hippocampus ( $P < .05$ ; Figure S3D).

In summary, PA reduces cerebrovascular activity in the hippocampus and cortex to chow levels and increases the number of GLUT-1+ particles per  $\text{mm}^2$ , reflecting vascular density, and GLUT-1 intensity, a marker for the amount of GLUT-1 transporters, in the hippocampus.<sup>51</sup>

### 3.7 | PA reverts HFD-induced effects in functional connectivity and microstructural gray and white matter integrity

To gain insight into functional and microstructural brain changes in HFD-induced obesity and the effects of CA and PA thereupon, mitochondrial enzyme activity analysis, rs-fMRI, and DTI were performed.

Cerebellar mitochondrial CS enzyme activity was comparable in all groups and the activity of complexes (I–IV) were unaffected by the treatments (Figure S4).

Functional connectivity was assessed by rs-fMRI using total and partial correlation analyses. Here, we observed no differences in functional connectivity, as analyzed with total correlations (Figure S5). Partial correlation highlights the direct connectivity between two regions. A reduction in partial functional connectivity was observed between the visual and auditory cortex in HFD mice compared to chow mice ( $P < .001$ ; Figure 6A,B). CA and PA had no effect on functional connectivity compared to HFD. However, the functional connectivity of CA and PA mice was comparable to chow mice ( $P > .05$ ), suggesting that CA and PA were able to revert the HFD-induced effects in functional connectivity.

Next, DTI was used to assess gray and white matter integrity in several brain regions. The FA was higher in HFD mice than in chow-fed mice in the somatosensory cortex ( $P < .05$ ) and visual cortex ( $P < .05$ ). No effects of CA or PA on the HFD-induced increase in FA levels in these brain regions were observed. However, FA levels of PA mice were comparable to chow ( $P > .05$ ), indicating that PA reverted the HFD-induced effects in the somatosensory cortex and visual cortex. Furthermore, HFD and CA had no effects on the FA in the hippocampus and motor cortex, but PA-treated mice had a significantly lower FA in the hippocampus ( $P < .01$ ) and motor cortex ( $P < .05$ ; Figure 6C) than HFD mice. The FA in these regions in PA mice was comparable to chow (both regions  $P > .05$ ).

The mean diffusivity (MD) in the hippocampus, motor cortex, somatosensory cortex and visual cortex were not affected by HFD (relative to chow), CA and PA (relative

to HFD) (Figure 6D). MD in the optic tract was significantly lower in HFD-fed animals than in chow-fed animals ( $P < .001$ , Figure 6D). CA and PA did not affect MD relative to HFD in any of the regions assessed. However, MD did not differ between PA-fed mice and chow mice in the optic tract ( $P > .05$ ), suggesting that PA reverted the HFD-induced effects on the MD in this region.

Taken together, CA and PA were able to revert the HFD-induced effects in functional connectivity between the visual and auditory cortex. PA altered microstructural gray matter integrity in the hippocampus and motor cortex, but this was not significant when compared to chow. In addition, PA reverted the HFD-induced effects in the somatosensory cortex, visual cortex and optic tract.

### 3.8 | PA affects genes and upstream regulators involved in synaptogenesis and inflammation

Hippocampal gene expression was studied using qRT-PCR and a multiplex neuroinflammation panel. Post synaptic density marker *Psd95* mRNA levels did not differ between the experimental groups (Figure 7A). Also, no differences between chow, HFD and CA mice were observed in synaptophysin (*Syp1*) mRNA levels. A trend toward reduced expression of synaptophysin in the hippocampus was observed in mice that received PA ( $P = .055$  vs HFD; Figure 7B), however, this was not significant when compared to chow.

A more extensive gene profiling analysis using a neuroinflammation panel followed by an upstream regulator analysis and an enrichment analysis across biological pathways confirmed this effect. There were no significant changes in predicted activation state of upstream regulators between chow and HFD (Figure 7C; signaling downstream of IFNG and STAT1 was significantly enriched in HFD but did not reach the cut-off value for relevant inhibition or activation). PA inhibited specific upstream regulators important in synaptogenesis relative to HFD (eg, GH1, WNT3A, VEGFA, BDNF, EGF, JUN; see Figure 7C). PA also attenuated signaling of the N-methyl-D-aspartate (NMDA) receptor a post-synaptic glutamate receptor involved in excitatory neurotransmission, important for synaptic plasticity and memory function. In addition, PA inhibited inflammatory pathways downstream of for example, IL-1, IL-1B, IL17A, IL-33, CXCL12. The above findings are supported by canonical pathway analysis showing significant inhibition of synaptogenesis and glutamate receptor signaling, neuroinflammation and lipopolysaccharide (LPS)-stimulated mitogen-activated kinase (MAPK) signaling pathways by PA (all  $P < .05$ ).

Altogether, we found that PA treatment showed anti-inflammatory effects and reduced synaptogenesis and synaptic plasticity signaling.

## 4 | DISCUSSION

The present study examined the potential health effects of PA and CA treatment on obesity-induced liver fibrosis as

well as brain function and structure. Such effects have, to our knowledge, not been investigated so far and, in case of CA, there are no published studies in rodent models of diet-induced obesity, dysmetabolism, and inflammation.

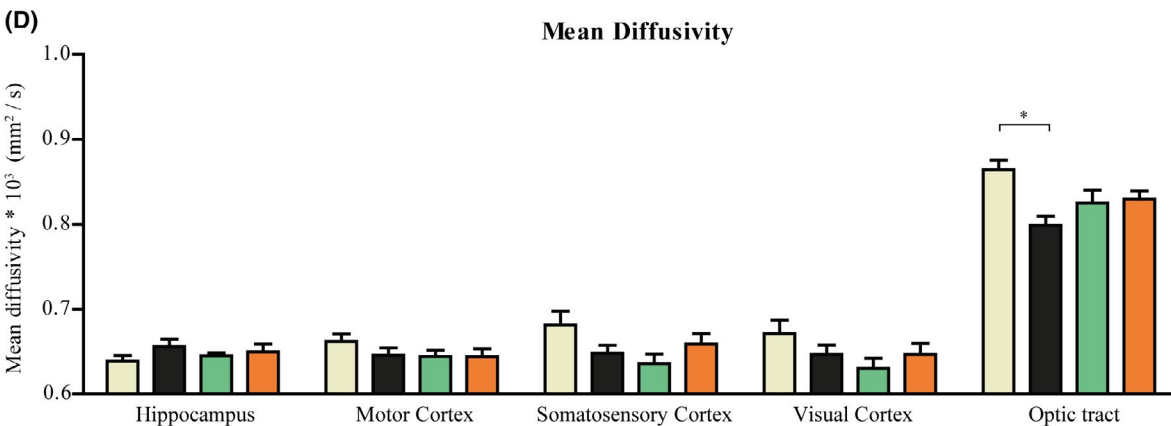
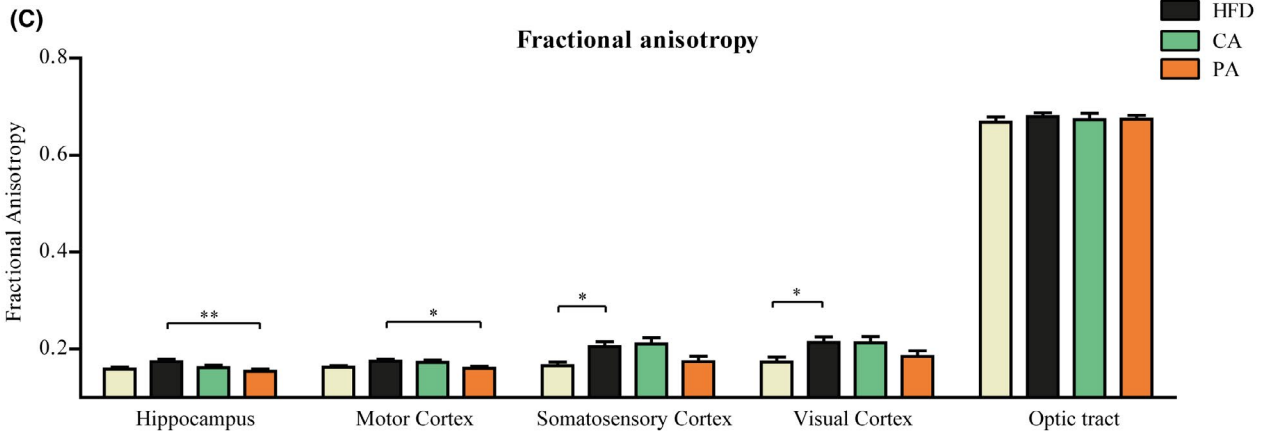
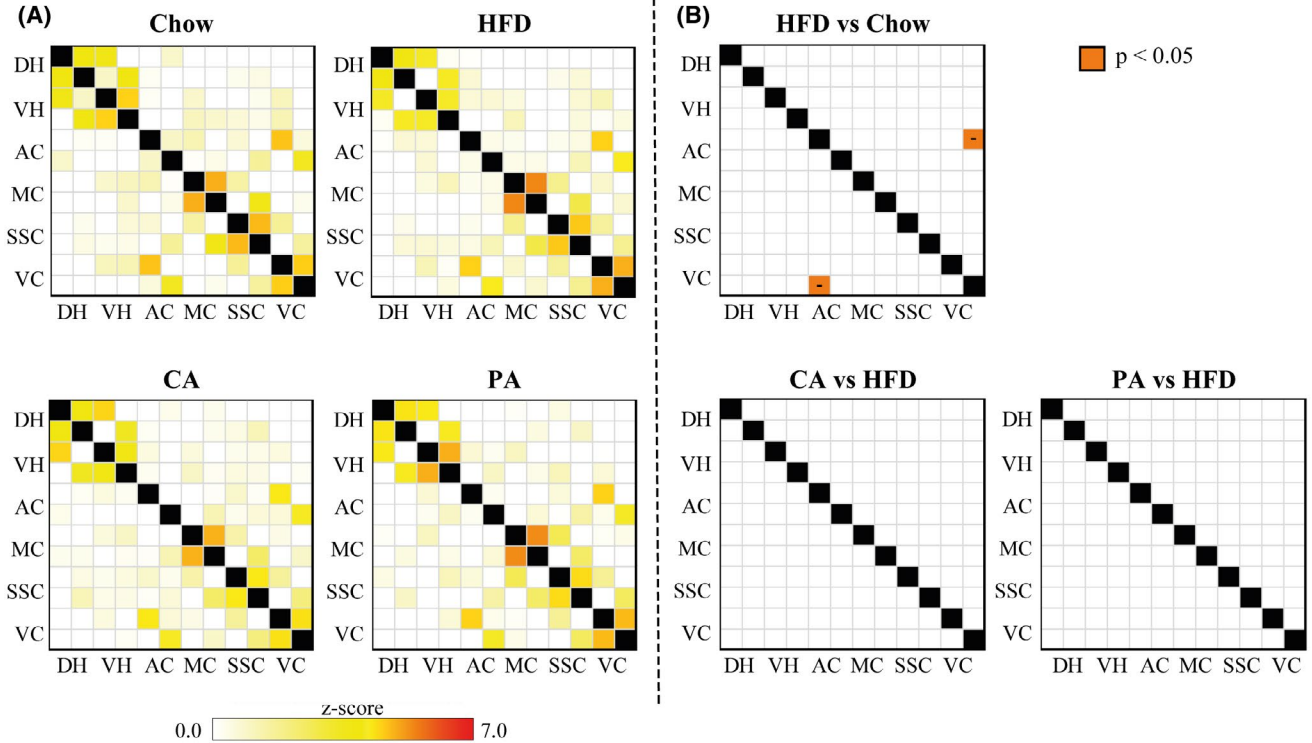


**FIGURE 6** Connectivity between brain regions and white matter integrity. A, Partial correlation matrixes of the Chow, HFD, CA, and PA experimental groups. The selected brain regions (dorsal hippocampus (DH), ventral hippocampus (VH), auditory cortex (AC), motor cortex (MC), somatosensory cortex (SSC), and visual cortex (VC) are subdivided in left hemisphere (first row) and right hemisphere (second row). A higher Z-score (red) indicates a stronger functional connectivity. B, Statistical analysis of functional connectivity between HFD and chow, CA and HFD, and PA and HFD. Minus (–) symbols in the matrix indicate whether the connectivity was decreased. Orange:  $P < .05$ . C, Differences in fractional anisotropy, and (D) mean diffusivity between the experimental groups in the hippocampus, motor cortex, somatosensory cortex, and visual cortex. Data are presented as mean  $\pm$  SEM, \* $P < .05$ , \*\* $P < .01$ . N = 14 (HFD) or N = 15 (chow, CA, PA) mice per group

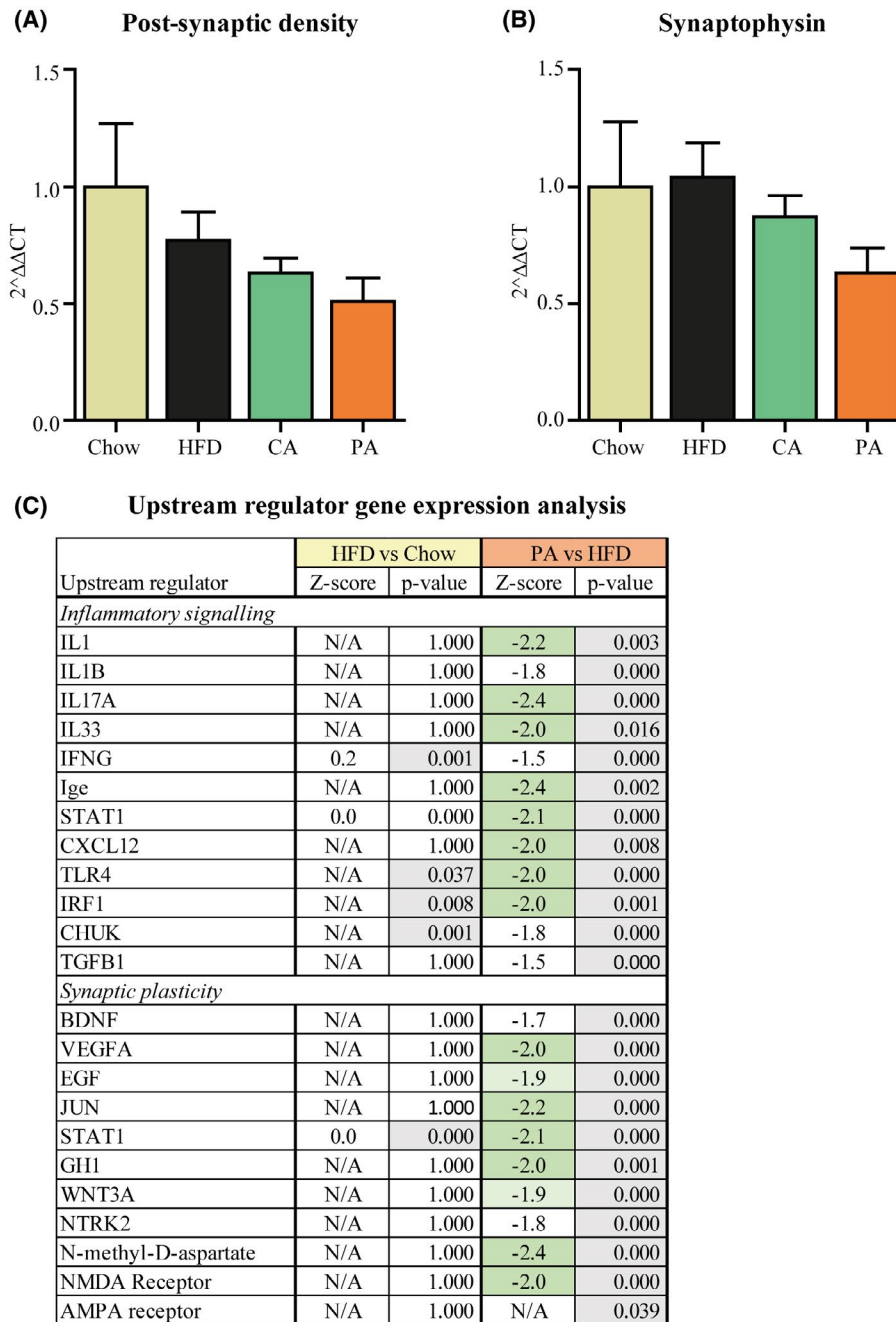


**FIGURE 7** Hippocampal synaptophysin, post-synaptic density, and upstream regulators. A, Post-synaptic density-95 and (B) Synaptophysin mRNA expression levels in the hippocampus. N = 14 (HFD) or N = 15 (chow, CA, PA) mice per group. C, Changes in upstream regulators are predicted from changes in transcription factors or key regulators with a Z-score.  $Z < -2$  indicates a relevant inhibition (shown in green) and  $Z > 2$  indicates a relevant activation. Significant changes with  $Z < -1.96$  are shown in light green. N/A indicates an insufficient number of differentially expressed genes to link gene effects to an upstream regulator. The p-value indicates significant enrichment of the genes downstream of a regulator. N = 8 per group. Data are presented as mean  $\pm$  SEM

In the present study, CA treatment showed no significant effects on body weight, plasma lipids, and metabolic risk factors as well as on liver steatosis. Interestingly, HFD treatment strongly lowered the hepatic glycogen content, and both CA and PA significantly prevented this reduction indicating an effect of both CA and PA on liver metabolism. A reduction in hepatic glycogen content appears to be indicative of a defect in liver metabolism, impaired liver function, and hepatic insulin resistance as reported by others,<sup>52,53</sup> an effect that has not been reported earlier in the HFD-fed *Ldlr*<sup>-/-</sup>.Leiden model of NASH. The hepatic glycogen augmenting effect of CA was paralleled by an insignificant reduction of lobular inflammation (by about 50%), whereas similar increases of hepatic glycogen with PA were associated with a reduction in liver inflammation. Because hepatic glycogen content is usually not determined in rodent studies of NAFLD/NASH, it is unclear whether the two effects are related to each other. It is well established that chronic tissue inflammation can impair insulin signaling, thereby, contributing to hepatic insulin resistance. It is thus possible that the observed increase in hepatic glycogen, the formation of which requires insulin signaling, is secondary to a possible inflammation-quenching effect of CA.

In contrast to CA, PA treatment prevented further HFD-induced weight gain independent of food intake. The attenuating effect on body weight as well as the reduction in plasma insulin levels observed here, are in line with the study of Lin et al in which a similar dose of 2.2% w/w PA was used.<sup>21</sup>

In addition, we observed that HFD increases SBP, a finding that is consistent with earlier studies.<sup>6,54</sup> PA-treatment was able to reduce the HFD-induced increased SBP, which is in line with observations in two other mouse models<sup>55</sup> and may be attributable to PA-induced endothelium-dependent vasodilation, as been previously reported in tail arteries.<sup>56</sup> Since high SBP is associated with high body weight<sup>57</sup>; and cognitive decline in humans,<sup>58</sup> the observed effects of PA on SBP and body weight may reduce the risk for cognitive decline.

The attenuating effects of PA treatment on obesity and metabolic risk factors are associated with a reduction in hepatic steatosis, accompanied by a reduction in hepatic CE content. These findings are in line with a previous study which showed reduced intrahepatic lipid accumulation in NAFLD patients (assessed by magnetic resonance imaging) upon increased colonic PA levels<sup>17</sup> and with *in vitro*<sup>59,60</sup> and *in vivo*<sup>18</sup> studies which show inhibition of lipid synthesis by PA. An alternative explanation for the observed antisteatotic effects of PA could be a stimulation of  $\beta$ -oxidation by PA, as has been previously reported in a short-term mouse study.<sup>18</sup> However we did not observe any effect of PA on hepatic  $\beta$ -hydroxybutyrate, a marker for  $\beta$ -oxidation, indicating that this pathway is not of major importance in the current study. Discrepancies between our findings and those of den Besten

et al could be due to differences in mouse strain and diet, lower dosage of PA used in our study (2.5% w/w), the therapeutic setting used here or the difference in methods used to measure  $\beta$ -oxidation.

PA also showed pronounced effects on hepatic inflammatory aggregates and collagen content, showing that PA can reduce development of NASH and liver fibrosis. To the best of our knowledge we are the first to comprehensively study the effects of PA on liver steatosis, inflammation, and fibrosis. Anti-inflammatory effects of PA have been reported previously for other organs and pathologies, such as acute leukemia,<sup>61</sup> cardiovascular disease<sup>55,62</sup> and inflammatory bowel disease<sup>63</sup> although the underlying mechanisms remain unclear.

To assess effects of PA and CA on behavior and cognition, we performed behavioral and cognitive tests. We found that HFD-fed mice had reduced motor coordination in the rotarod test. CA and PA could not reverse this effect. PA mice spent more time in the corners of the open field test than chow mice, suggesting that PA mice were more anxious than chow-fed mice. Increased anxiety-like behavior after PA administration has been reported in other studies as well.<sup>64-66</sup> Exploration activity and spatial learning and memory were not affected by HFD, CA, or PA. Other studies found cognitive deficits, increased motor activity, and impaired spatial memory in rats that were given PA.<sup>67-69</sup> However, these rats were given PA via intracerebroventricular injections with a relatively high dosage (4  $\mu$ L of 0.26 M) of PA.

We measured cerebral vasoreactivity, a measure of ability to respond to vasoconstrictive stimuli, to study the effects of PA and CA on cerebrovascular health. Overall, the cerebral vasoreactivity levels that we detected, are similar to those found in another study.<sup>34</sup>

The cerebral vasoreactivity levels in the cortex and hippocampus were very low in HFD compared to chow, albeit not significant (cortex:  $P = .089$ ; hippocampus:  $P = .100$ ). HFD-induced obesity is associated with cerebrovascular remodeling,<sup>70,71</sup> an active process of structural changes of the vessel wall.<sup>72</sup> These structural changes to the vasculature can result in a decreased diameter of the blood vessels, and can lead to an exaggerated response to vasoconstrictive stimuli.<sup>73</sup> Hypertension can induce hyperperfusion of (brain) tissue, which is then followed by remodeling of the vasculature.<sup>73</sup> Moreover, hypertension and obesity are associated with rarefaction (a loss of capillaries and arterioles), which further contributes to vascular remodeling.<sup>73,74</sup> In line with this, the relative GLUT-1+ area in the thalamus was decreased in HFD mice compared to chow. GLUT-1 is selectively expressed in the cerebral capillary endothelium, and is used as a marker for cerebrovascular integrity.<sup>34</sup> This indicates that HFD is able to affect cerebrovascular integrity.

PA reverted HFD-induced effects on cerebrovascular activity in the hippocampus and cortex to chow levels. This

adapted cerebral vasoreactivity is in line with the increased hippocampal GLUT-1, and may explain the effects of PA on cerebral hemodynamics. Together, this suggests that PA is able to revert HFD-induced vascular remodeling.

We revealed that PA reversed the HFD-induced effect mainly in different components of the visual system, that is, the visual cortex and the optic tract. HFD decreased functional connectivity between the visual cortex and the auditory cortex, an effect that was reversed by CA and PA. Moreover, HFD mice had a higher FA in cortical regions, that is, the visual and somatosensory cortex, and a lower MD in the optic tract compared to chow mice. PA treatment reduced FA in the visual and somatosensory cortex, and increased MD in the optic tract, which could suggest that PA reversed the HFD-induced effects back to chow or prevented further changes upon start of PA treatment. Recent studies by Medic et al and Ou et al, described positive associations between white matter integrity and increased adiposity.<sup>75,76</sup> In addition, we revealed possible negative effects of PA on synaptogenesis in the hippocampus. Gene expression analysis in the hippocampus showed that synaptic signaling was reduced and associated with a reduction of glutamate signaling and upstream regulator NMDA in PA mice. Neuronal glutamate signaling is vital for the encoding of information, the formation and retrieval of memories, spatial recognition and the maintenance of consciousness.<sup>77</sup> NMDA receptors are involved in myelinating processes, and consistent herewith, NMDA receptor antagonists, like memantine and MK801, have shown a decrease in FA in the hippocampus of rats.<sup>78,79</sup>

In conclusion, we found that PA exerted pronounced positive effects on metabolic risk factors and attenuated the development of HFD-induced NASH and liver fibrosis. PA also decreased the systolic blood pressure and reverted cerebral vasoreactivity. PA reverted HFD-induced effects in functional connectivity and microstructural gray and white matter integrity to chow levels, however PA also increased anxiety-like behavior and reduced regulation of synaptogenesis in the hippocampus. Therefore, caution should be used when considering PA as treatment, even though positive effects on metabolism, (cerebro) vasculature, and on both brain structure and function were observed.

## ACKNOWLEDGMENTS

We thank the bio-technicians at TNO Metabolic Health Research and at the Animal Research Facility of the Radboud university medical center for taking excellent care of the mice. We also thank Andor Veltien, Sjaak van Asten, and Tim Emmerzaal for their great scientific support. This study was supported by the TNO Early Research Program 'Body Brain Interactions'.

## CONFLICT OF INTEREST

The authors declare no conflicts of interest.

## AUTHOR CONTRIBUTIONS

A.J. Kiliaan, M.C. Morrison, R. Kleemann, and T. Kozicz contributed to the conception of the study. A.C. Tengeler, E. Gart, M. Wiesmann, and I.A.C. Arnoldussen contributed to the design of the study. A.C. Tengeler, E. Gart, M. Wiesmann, I.A.C. Arnoldussen, W. van Duyvenvoorde, M. Hoogstad, P.J. Dederen, V. Verweij and B. Geenen contributed to the acquisition and analysis of the data. A.C. Tengeler, E. Gart, M. Wiesmann, A.J. Kiliaan, M.C. Morrison, R. Kleemann, and T. Kozicz contributed to drafting and critically revising the manuscript. All authors read and approved the final version before submission.

## REFERENCES

1. Ng M, Fleming T, Robinson M, et al. Global, regional, and national prevalence of overweight and obesity in children and adults during 1980–2013: a systematic analysis for the Global Burden of Disease Study 2013. *Lancet*. 2014;384:766-781.
2. Burhans MS, Hagman DK, Kuzma JN, Schmidt KA, Kratz M. Contribution of adipose tissue inflammation to the development of type 2 diabetes mellitus. *Compr Physiol*. 2018;9:1-58.
3. Kitade H, Chen G, Ni Y, Ota T. Nonalcoholic fatty liver disease and insulin resistance: new insights and potential new treatments. *Nutrients*. 2017;9(4):387.
4. Friedman SL, Neuschwander-Tetri BA, Rinella M, Sanyal AJ. Mechanisms of NAFLD development and therapeutic strategies. *Nat Med*. 2018;24:908-922.
5. Bataller R, Brenner DA. Liver fibrosis. *J Clin Invest*. 2005;115:209-218.
6. Arnoldussen IAC, Wiesmann M, Pelgrim CE, et al. Butyrate restores HFD-induced adaptations in brain function and metabolism in mid-adult obese mice. *Int J Obes (Lond)*. 2017;41:935-944.
7. de Mello AH, Costa AB, Engel JDG, Rezin GT. Mitochondrial dysfunction in obesity. *Life Sci*. 2018;192:26-32.
8. Pannacciulli N, Del Parigi A, Chen K, Le DS, Reiman EM, Tataranni PA. Brain abnormalities in human obesity: a voxel-based morphometric study. *NeuroImage*. 2006;31:1419-1425.
9. van Bloemendaal L, Ijzerman RG, Ten Kulve JS, et al. Alterations in white matter volume and integrity in obesity and type 2 diabetes. *Metab Brain Dis*. 2016;31:621-629.
10. Uraga RM, Keller JN. The complex interactions between obesity, metabolism and the brain. *Front Neurosci*. 2019;13:513.
11. Hurr C, Patik JC, Kim K, Brothers RM. Blunted cerebral vascular responsiveness to hypercapnia in obese individuals. *Exp Physiol*. 2017;102:1300-1308.
12. Jais A, Solas M, Backes H, et al. Myeloid-cell-derived VEGF maintains brain glucose uptake and limits cognitive impairment in obesity. *Cell*. 2016;165:882-895.
13. Mar Rodriguez M, Perez D, Javier Chaves F, et al. Obesity changes the human gut mycobiome. *Sci Rep*. 2015;5:14600.
14. Patrone V, Vajana E, Minuti A, et al. Postoperative changes in fecal bacterial communities and fermentation products in obese patients undergoing bilio-intestinal bypass. *Front Microbiol*. 2016;7:200.
15. Rial SA, Ravaut G, Malaret TB, Bergeron KF, Mounier C. Hexanoic, octanoic and decanoic acids promote basal and insulin-induced phosphorylation of the Akt-mTOR axis and a balanced

- lipid metabolism in the HepG2 hepatoma cell line. *Molecules*. 2018;23:2315.
16. Akpa MM, Point F, Sawadogo S, Radenne A, Mounier C. Inhibition of insulin and T3-induced fatty acid synthase by hexanoate. *Lipids*. 2010;45:997-1009.
  17. Chambers E, Viardot A, Psichas A, et al. Effects of elevating colonic propionate on liver fat content in overweight adults with non-alcoholic fatty liver disease: a pilot study. *Proc Nutr Soc*. 2015;74.
  18. den Besten G, Bleeker A, Gerding A, et al. Short-chain fatty acids protect against high-fat diet-induced obesity via a PPARgamma-dependent switch from lipogenesis to fat oxidation. *Diabetes*. 2015;64:2398-2408.
  19. De Vadder F, Kovatcheva-Datchary P, Goncalves D, et al. Microbiota-generated metabolites promote metabolic benefits via gut-brain neural circuits. *Cell*. 2014;156:84-96.
  20. Chambers ES, Preston T, Frost G, Morrison DJ. Role of gut microbiota-generated short-chain fatty acids in metabolic and cardiovascular health. *Curr Nutr Rep*. 2018;7:198-206.
  21. Lin HV, Frassetto A, Kowalik EJ Jr, et al. Butyrate and propionate protect against diet-induced obesity and regulate gut hormones via free fatty acid receptor 3-independent mechanisms. *PLoS One*. 2012;7:e35240.
  22. Takai A, Kikuchi K, Ichimura M, et al. Fructo-oligosaccharides ameliorate steatohepatitis, visceral adiposity, and associated chronic inflammation via increased production of short-chain fatty acids in a mouse model of non-alcoholic steatohepatitis. *BMC Gastroenterol*. 2020;20:46.
  23. Morrison MC, Verschuren L, Salic K, et al. Obeticholic acid modulates serum metabolites and gene signatures characteristic of human NASH and attenuates inflammation and fibrosis progression in Ldlr-/-Leiden mice. *Hepatol Commun*. 2018;2:1513-1532.
  24. Kilkenny C, Browne WJ, Cuthi I, Emerson M, Altman DG. Improving bioscience research reporting: the ARRIVE guidelines for reporting animal research. *Vet Clin Pathol*. 2012;41:27-31.
  25. Liang W, Menke AL, Driessen A, et al. Establishment of a general NAFLD scoring system for rodent models and comparison to human liver pathology. *PLoS One*. 2014;9:e115922.
  26. Bligh EG, Dyer WJ. A rapid method of total lipid extraction and purification. *Can J Biochem Physiol*. 1959;37:911-917.
  27. Galarraga M, Champion J, Munoz-Barrutia A, et al. Adiposoft: automated software for the analysis of white adipose tissue cellularity in histological sections. *J Lipid Res*. 2012;53:2791-2796.
  28. Schindelin J, Arganda-Carreras I, Frise E, et al. Fiji: an open-source platform for biological-image analysis. *Nat Methods*. 2012;9:676-682.
  29. Schneider CA, Rasband WS, Eliceiri KW. NIH image to imageJ: 25 years of image analysis. *Nat Methods*. 2012;9:671-675.
  30. Mulder P, Morrison MC, Wielinga PY, van Duyvenvoorde W, Kooistra T, Kleemann R. Surgical removal of inflamed epididymal white adipose tissue attenuates the development of non-alcoholic steatohepatitis in obesity. *Int J Obes (Lond)*. 2016;40:675-684.
  31. Pernold K, Iannello F, Low BE, et al. Towards large scale automated cage monitoring - Diurnal rhythm and impact of interventions on in-cage activity of C57BL/6J mice recorded 24/7 with a non-disrupting capacitive-based technique. *PLoS One*. 2019;14:e0211063.
  32. Giles JM, Whitaker JW, Moy SS, Fletcher CA. Effect of environmental enrichment on aggression in BALB/cJ and BALB/cByJ mice monitored by using an automated system. *J Am Assoc Lab Anim Sci*. 2018.
  33. Wiesmann M, Zerbi V, Jansen D, et al. Hypertension, cerebrovascular impairment, and cognitive decline in aged AbetaPP/PS1 mice. *Theranostics*. 2017;7:1277-1289.
  34. Arnoldussen IAC, Zerbi V, Wiesmann M, et al. Early intake of long-chain polyunsaturated fatty acids preserves brain structure and function in diet-induced obesity. *J Nutr Biochem*. 2016;30:177-188.
  35. Zerbi V, Jansen D, Wiesmann M, et al. Multinutrient diets improve cerebral perfusion and neuroprotection in a murine model of Alzheimer's disease. *Neurobiol Aging*. 2014;35:600-613.
  36. Zerbi V, Wiesmann M, Emmerzaal TL, et al. Resting-state functional connectivity changes in aging apoE4 and apoE-KO mice. *J Neurosci*. 2014;34:13963-13975.
  37. Harsan L-A, Paul D, Schnell S, et al. In vivo diffusion tensor magnetic resonance imaging and fiber tracking of the mouse brain. *NMR Biomed*. 2010;23:884-896.
  38. Alexander AL, Lee JE, Lazar M, Field AS. Diffusion tensor imaging of the brain. *Neurotherapeutics*. 2007;4:316-329.
  39. Paxinos G, Franklin K. *Paxinos and Franklin's the Mouse Brain in Stereotaxic Coordinates*. London: Academic Press; 2001.
  40. Wiesmann M, Zinnhardt B, Reinhardt D, et al. A specific dietary intervention to restore brain structure and function after ischemic stroke. *Theranostics*. 2017;7:493-512.
  41. Janssen AJ, Trijbels FJ, Sengers RC, et al. Spectrophotometric assay for complex I of the respiratory chain in tissue samples and cultured fibroblasts. *Clin Chem*. 2007;53:729-734.
  42. Emmerzaal TL, Rodenburg RJ, Tanila H, Verweij V, Kiliaan AJ, Kozicz T. Age-dependent decrease of mitochondrial complex II activity in a familial mouse model for Alzheimer's disease. *J Alzheimers Dis*. 2018;66:75-82.
  43. Srere PA. [1] Citrate synthase: [EC 4.1.3.7. Citrate oxaloacetate-lyase (CoA-acetylating)]. In *Methods in Enzymology*, Vol. 13. London: Academic Press; 1969:3-11.
  44. Janssen CIF, Zerbi V, Mutsaers MPC, et al. Impact of dietary n-3 polyunsaturated fatty acids on cognition, motor skills and hippocampal neurogenesis in developing C57BL/6J mice. *J Nutr Biochem*. 2015;26:24-35.
  45. Pfaffl MW. A new mathematical model for relative quantification in real-time RT-PCR. *Nucleic Acids Res*. 2001;29:e45.
  46. Liang W, Tonini G, Mulder P, et al. Coordinated and interactive expression of genes of lipid metabolism and inflammation in adipose tissue and liver during metabolic overload. *PLoS One*. 2013;8:e75290.
  47. Wiesmann M, Roelofs M, van der Lugt R, Heerschap A, Kiliaan AJ, Claassen JA. Angiotensin II, hypertension and angiotensin II receptor antagonism: Roles in the behavioural and brain pathology of a mouse model of Alzheimer's disease. *J Cereb Blood Flow Metab*. 2017;37:2396-2413.
  48. Vani K, Sompuram SR, Schaedle AK, et al. The importance of epitope density in selecting a sensitive positive IHC control. *J Histochem Cytochem*. 2017;65:463-477.
  49. Uhlar CM, Whitehead AS. Serum amyloid A, the major vertebrate acute-phase reactant. *Eur J Biochem*. 1999;265:501-523.
  50. Samuel VT, Liu Z-X, Qu X, et al. Mechanism of hepatic insulin resistance in non-alcoholic fatty liver disease. *J Biol Chem*. 2004;279:32345-32353.
  51. Choeiri C, Staines W, Messier C. Immunohistochemical localization and quantification of glucose transporters in the mouse brain. *Neuroscience*. 2002;111:19-34.
  52. Wagner J, Fillebeen C, Haliotis T, et al. Mouse models of hereditary hemochromatosis do not develop early liver fibrosis in response to a high fat diet. *PLoS One*. 2019;14:e0221455.

53. Xu H, Zhou Y, Liu Y, et al. Metformin improves hepatic IRS2/PI3K/Akt signaling in insulin-resistant rats of NASH and cirrhosis. *J Endocrinol*. 2016;229:133-144.
54. de Montgolfier O, Pouliot P, Gillis MA, Ferland G, Lesage F, Thorin-Trescases N, Thorin E. Systolic hypertension-induced neurovascular unit disruption magnifies vascular cognitive impairment in middle-age atherosclerotic LDLr(-/-):hApoB(+/-) mice. *Geroscience*. 2019;41:511-532.
55. Bartolomeaus H, Balogh A, Yakoub M, et al. Short-chain fatty acid propionate protects from hypertensive cardiovascular damage. *Circulation*. 2019;139:1407-1421.
56. Natarajan N, Hori D, Flavahan S, et al. Microbial short chain fatty acid metabolites lower blood pressure via endothelial G protein-coupled receptor 41. *Physiol Genomics*. 2016;48:826-834.
57. Seravalle G, Grassi G. Obesity and hypertension. *Pharmacol Res*. 2017;122:1-7.
58. Lopez OL, Jagust WJ, Dulberg C, et al. Risk factors for mild cognitive impairment in the Cardiovascular Health Study Cognition Study: part 2. *Arch Neurol*. 2003;60:1394-1399.
59. Demigne C, Morand C, Levrat MA, Besson C, Moundras C, Remesy C. Effect of propionate on fatty acid and cholesterol synthesis and on acetate metabolism in isolated rat hepatocytes. *Br J Nutr*. 1995;74:209-219.
60. Wright RS, Anderson JW, Bridges SR. Propionate inhibits hepatocyte lipid synthesis. *Proc Soc Exp Biol Med*. 1990;195:26-29.
61. Bindels LB, Porporato P, Dewulf EM, et al. Gut microbiota-derived propionate reduces cancer cell proliferation in the liver. *Br J Cancer*. 2012;107:1337-1344.
62. Li M, van Esch B, Wagenaar GTM, Garssen J, Folkerts G, Henricks PAJ. Pro- and anti-inflammatory effects of short chain fatty acids on immune and endothelial cells. *Eur J Pharmacol*. 2018;831:52-59.
63. Tedelind S, Westberg F, Kjerrulf M, Vidal A. Anti-inflammatory properties of the short-chain fatty acids acetate and propionate: a study with relevance to inflammatory bowel disease. *World J Gastroenterol*. 2007;13:2826-2832.
64. Foley KA, Ossenkopp K-P, Kavaliers M, MacFabe DF. Pre- and neonatal exposure to lipopolysaccharide or the enteric metabolite, propionic acid, alters development and behavior in adolescent rats in a sexually dimorphic manner. *PLoS One*. 2014;9:e87072.
65. Wah DTO, Ossenkopp K-P, Bishnoi I, Kavaliers M. Predator odor exposure in early adolescence influences the effects of the bacterial product, propionic acid, on anxiety, sensorimotor gating, and acoustic startle response in male rats in later adolescence and adulthood. *Physiol Behav*. 2019;199:35-46.
66. Shams S, Foley KA, Kavaliers M, MacFabe DF, Ossenkopp K-P. Systemic treatment with the enteric bacterial metabolic product propionic acid results in reduction of social behavior in juvenile rats: contribution to a rodent model of autism spectrum disorder. *Dev Psychobiol*. 2019;61:688-699.
67. Shultz SR, MacFabe DF, Ossenkopp K-P, et al. Intracerebroventricular injection of propionic acid, an enteric bacterial metabolic end-product, impairs social behavior in the rat: implications for an animal model of autism. *Neuropharmacology*. 2008;54:901-911.
68. MacFabe DF, Cain NE, Boon F, Ossenkopp K-P, Cain DP. Effects of the enteric bacterial metabolic product propionic acid on object-directed behavior, social behavior, cognition, and neuroinflammation in adolescent rats: Relevance to autism spectrum disorder. *Behav Brain Res*. 2011;217:47-54.
69. MacFabe DF, Cain DP, Rodriguez-Capote K, et al. Neurobiological effects of intraventricular propionic acid in rats: possible role of short chain fatty acids on the pathogenesis and characteristics of autism spectrum disorders. *Behav Brain Res*. 2007;176:149-169.
70. Deutsch C, Portik-Dobos V, Smith AD, Ergul A, Dorrance AM. Diet-induced obesity causes cerebral vessel remodeling and increases the damage caused by ischemic stroke. *Microvasc Res*. 2009;78:100-106.
71. Deng J, Zhang J, Feng C, Xiong L, Zuo Z. Critical role of matrix metalloproteinase-9 in chronic high fat diet-induced cerebral vascular remodelling and increase of ischaemic brain injury in mice. *Cardiovasc Res*. 2014;103:473-484.
72. Renna NF, de Las Heras N, Miatello RM. Pathophysiology of vascular remodeling in hypertension. *Int J Hypertens*. 2013;2013:808353.
73. Jennings JR, Zanstra Y. Is the brain the essential in hypertension? *NeuroImage*. 2009;47:914-921.
74. Sorop O, Olver TD, van de Wouw J, et al. The microcirculation: a key player in obesity-associated cardiovascular disease. *Cardiovasc Res*. 2017;113:1035-1045.
75. Medic N, Kochunov P, Ziauddeen H, et al. BMI-related cortical morphometry changes are associated with altered white matter structure. *Int J Obes (Lond)*. 2019;43:523-532.
76. Ou X, Andres A, Pivik RT, Cleves MA, Badger TM. Brain gray and white matter differences in healthy normal weight and obese children. *J Magn Reson Imaging*. 2015;42:1205-1213.
77. Daikhin Y, Yudkoff M. Compartmentation of brain glutamate metabolism in neurons and glia. *J Nutr*. 2016;146:1026S-1031S.
78. Sekar S, Jonckers E, Verhoye M, et al. Subchronic memantine induced concurrent functional disconnectivity and altered ultra-structural tissue integrity in the rodent brain: revealed by multimodal MRI. *Psychopharmacology*. 2013;227:479-491.
79. Wu H, Wang X, Gao Y, et al. NMDA receptor antagonism by repetitive MK801 administration induces schizophrenia-like structural changes in the rat brain as revealed by voxel-based morphometry and diffusion tensor imaging. *Neuroscience*. 2016;322:221-233.

## SUPPORTING INFORMATION

Additional Supporting Information may be found online in the Supporting Information section.

**How to cite this article:** Tengeler AC, Gart E, Wiesmann M, et al. Propionic acid and not caproic acid, attenuates nonalcoholic steatohepatitis and improves (cerebro) vascular functions in obese Ldlr<sup>-/-</sup>. Leiden mice. *The FASEB Journal*. 2020;00:1-19. <https://doi.org/10.1096/fj.202000455R>